

A SMART CONTROLLABLE SMA-BASED TOURNIQUET

Alireza Golgouneh¹, Jiaqi Li², Julianna Abel², and Lucy E. Dunne³

1. Department of Electrical and Computer Engineering

2. Department of Mechanical Engineering

3. Department of Design, Housing, and Apparel

University of Minnesota-Twin Cities, Minneapolis, MN, USA

ABSTRACT

Textile-based compression devices are widely used in fields such as healthcare, astronautics, cosmetics, defense, and more. While traditional compression garments are only able to apply passive pressure on the body, there have been some efforts to integrate smart materials such as shape memory alloys (SMAs) to make compression garments active and controllable. However, despite the advances in this field, accurate control of applied pressure on the body due remains a challenge due to vast population-scale anthropometric variability and intra-subjects variability in tissue softness, even if the actuators themselves are fully characterized. In this study, we begin to address these challenges by developing a novel size-adjustable SMA-based smart tourniquet capable of producing a controllable pressure for circumferential applications. The developed prototype was tested on an inflatable pressure cuff wrapped around a rigid cylinder. The thermal activation of SMA coils was achieved through Joule heating, and a microcontroller and a programmable power supply are used to provide the input signal. To control the compression force, a closed-loop PID controller was implemented, and the performance of the system was evaluated in 5 different testing conditions for variable and cyclic compression levels. The experiments showed that the controlled system could follow the desired control pressure reference with a steady-state of 1 mmHg. The compression tourniquet is able to produce more than 33 mmHg with an average actuation rate of 0.19 mmHg/s. This is the first demonstration of accurate closed-loop control of an SMA-incorporated compression technology to the best of our knowledge. This paper enables new, dynamic systems with controllable activation and low-effort donning and doffing, with applications ranging from healthcare solutions to advanced spacesuit design.

Keywords: Shape Memory Alloy, Smart Tourniquet, Closed Loop Control

1. INTRODUCTION

Compression garments are widely used for various applications in medical therapy, aerospace and astronautics, and cosmetics, among other fields. For instance, compression therapy is used for the treatment of various conditions such as lymphedema, diabetes, venous insufficiency, and skin burns [1]. Compression devices are also used in the astronautics and aerospace engineering field to simulate the earth's atmospheric pressure in Mechanical Counter-Pressure (MCP) suits [2,3]. In the athletic field, compression garments are worn to improve athletic performance. Traditionally, passive compression garments are made of elastic textiles, and they are typically made undersized to provide passive compression on the body. One of the commonly-used mechanisms of providing active compression is pneumatic inflatable bladder systems that actively change garment dimensions, and consequently, applied pressure [4]. However, these systems are primarily bulky and require air pumps, which are prone to leaks and may result in pressure drop after long-term use [5].

The use of active materials could be a viable alternative to pneumatic-based compression systems. The term "active materials" refers here to materials with shape memory functions that can retain a specific shape after certain external stimuli. These materials include (but are not limited to) shape memory alloys (SMAs), shape memory polymers (SMPs), piezoelectric ceramics, ionic polymer metal composites, and dielectric elastomer actuators (DEAs). Although these materials have salient actuation features, they have some limitations preventing them from being fully practical for wearable applications [6].

Among these materials, the most outstanding performance and practicality are demonstrated by Nickel-Titanium (NiTi, also known as NiTiNol) SMAs. Compared to the other active materials, SMAs can generate periodic forces under thermal

stimulation. At the same time, SMA is lightweight, safe, and easy-to-embed with traditional fabrics. One of the problems of SMAs reported in previous studies is the problem of high austenite (actuation) temperature for certain SMAs [7]. However, this issue can be resolved by integrating appropriate heat-resistant fabrics such as Nomex to insulate it from directly being in touch with the skin surface. SMAs have recently been used in previous studies to apply pressure on the body in different geometrical configurations such as a tourniquet [6,8], and SMA-knitted compression garments [9,10]. However, despite the advances in this field, due to vast variability in population anthropometrics and tissue softness, the amount of pressure applied on the body by a compression device may vary significantly between wearers. As a result, these compression devices cannot automatically adjust the pressure. If the pressure is too low, the task goal may not be achieved, and if the pressure is too high, it may cause serious problems to the body [11]. One possible solution is embedding sensors to measure the applied pressure. These sensors, which for wearable applications are ideally textile-based, are associated with significant issues such as response drift, nonlinearity, etc. [12,13]. Therefore, some efforts have been made to replace these textile-based sensors with other materials such as dielectric elastomer [14] materials or optical fibers [15]. For instance, Goncalves et al. [6] have presented an active-controlled compression garment that integrates NiTi coil actuators and fiber optic strain sensors to produce dynamic compression. However, these sensors introduce other types of challenges which make them impractical for real-world applications.

One possible solution to overcome these challenges is closing the actuation loop by automatically feeding the sensor measurements back to the system and adjusting the pressure level. Implementing a closed-loop control has not yet been done for SMA-based compression devices. This paper develops a novel size-adjustable SMA-based smart tourniquet capable of producing a controllable pressure of more than 33 mmHg for circumferential applications. The system requirements and the compression tourniquet design are discussed. Then the sensors are modeled, and the maximum counter pressure is calculated based on the model presented by Holschuh et al. in [8]. Next, the controller is designed, and the criteria for selecting the controller gains are explained. Finally, the performance of the designed novel active-controlled compression tourniquet is evaluated by conducting experiments. This research establishes accurate closed-loop control of SMA-incorporated compression technology, which has the potential to enable diverse devices that require a controlled amount of pressure to be applied on the body, such as medical therapy, cosmetics, athletics, and aerospace engineering.

2. SYSTEM REQUIREMENTS AND DESIGN

2.1 Actuator Design

To manufacture the actuators, an approach presented and used in [8] was adopted. In this method, the SMA wire is shaped into a

coil to be then made into a spring via heat treatment. To manufacture the spring actuators, NiTi [Dynalloy Inc.] SMA wire with a thickness of 0.304 mm (0.012") was wound around 1.0414 mm (0.041") stainless-steel core (**Error! Reference source not found.**). The shape setting is done by heat treating the coils at 450°C for 10 minutes. Once heat-set, the coil is water quenched, and the austenite memory state of SMA is reset.

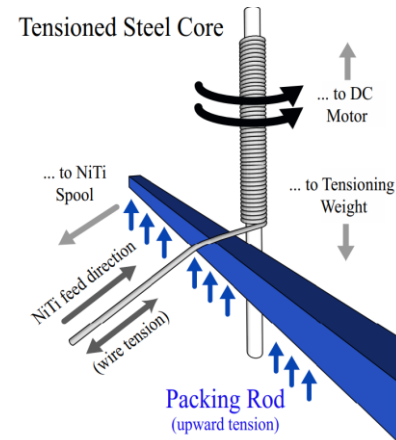


Figure 1: Winding method to manufacture the SMA spring coil actuators (inspired by [8]).

2.2 Prototype Design

The active compression garment was designed and developed by taking the following criteria into account:

- 1- Minimizing the compression area to maximize the compression level
- 2- Easily donning/doffing
- 3- Adjusting the passive and active compression
- 4- Controlling the actuation level
- 5- Minimizing the actuation loss by minimizing the fabric stretch and elasticity
- 6- Wearable, washable, comfortable

As illustrated in Figure 2 (a), this prototype consists of three subcomponents. The middle section consists of five separate parallel-aligned SMA springs that are attached to the other two sections with two 3/8" (0.95 cm) diameter brass-nickel alloy snaps. These snaps have two parts, stud and socket, which are fastened to make a detachable closure. The space between snap buttons enables replacing the actuators with different materials or lengths to achieve variable actuation results when needed. This also means the SMA actuators can be readily replaced without making any structural changes to the prototype when encountering actuation loss due to material fatigue, overheating, or excessive loading [8]. Moreover, the electrical conductivity of these snaps allows the SMA actuators to be connected in series configuration. With this configuration, all of the actuators can be activated using one power channel, and although the power

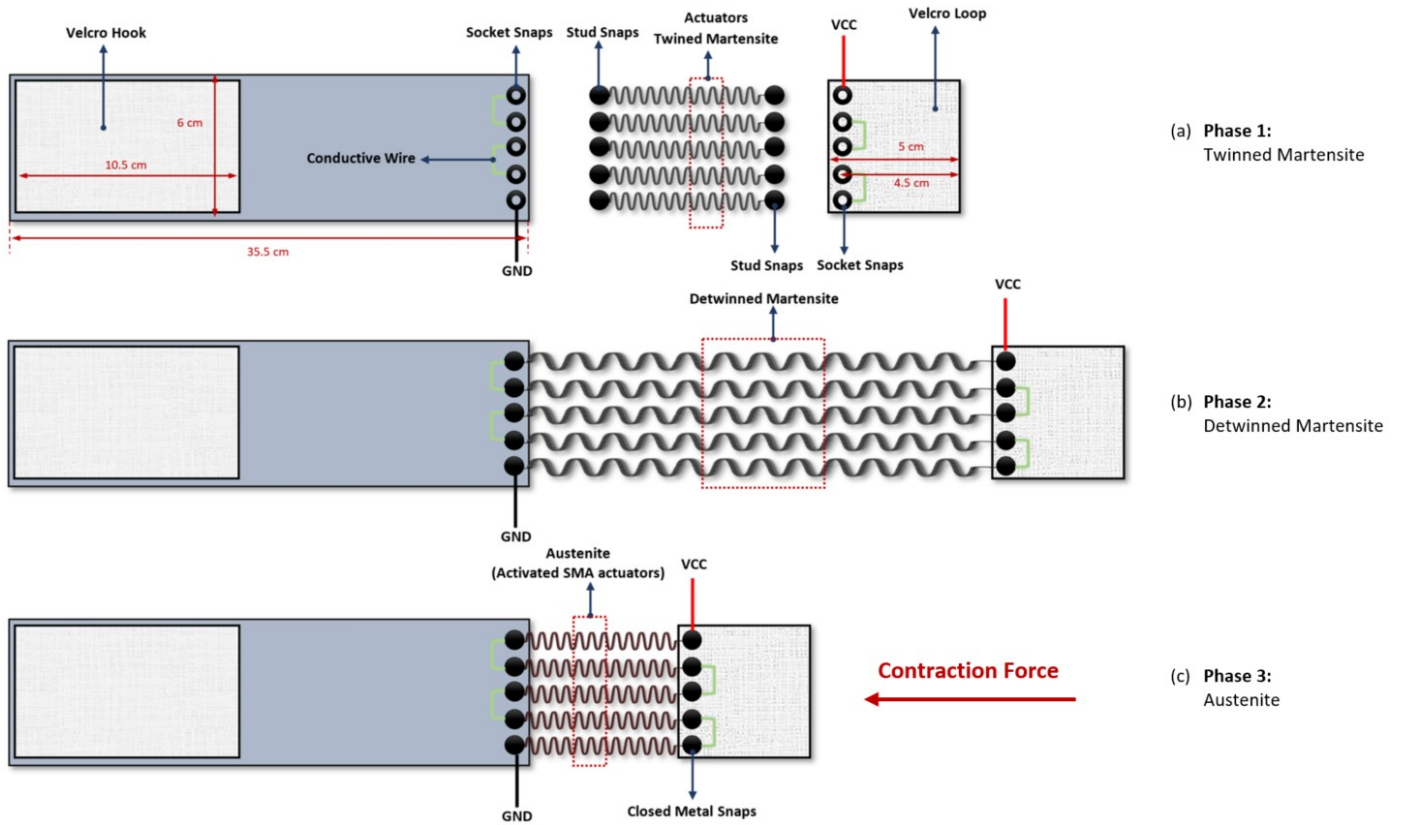


Figure 2: The schematic of the developed smart controllable SMA-based tourniquet showing the device components and the three activation phases of the SMA actuators: (a) Twinned Martensite, (b) Detwinned Martensite, and (c) Austenite

consumption is constant, they require less current compared to a parallel configuration. In addition, due to the vast anthropometric variability across the population, Velcro hook and loop strips were used to ensure that the prototype accurately fits around the desired body part, such as calf with different shapes and sizes. To prevent the prototype from being stretched and absorbing the compression generated by the SMA actuators, the 10.5 cm long Velcro hook was stitched to a 35.5 cm long, 6 cm wide, non-stretchable, and soft PVC Coated Tarpaulin fabric.

Therefore, with this mechanism, the active effective length of the tourniquet (L_e) (without considering the actuator length) can vary from 24 cm to 35.5 cm. As shown in Figure 2, while the SMA actuators are in the detwinned Martensite phase (un-actuated), the tourniquet can be stretched to be wrapped around an object. Once the SMA actuators are stimulated using the Joule heating approach (i.e., applying electrical power), the temperature of the actuators increases due to the phase transition from martensite to austenite, which leads to activation of the SMA coils and generation of the contraction force.

2.3 Experimental Setup

The actual experimental setup is shown in Figure 3 and Figure 4. As shown in these figures, an inflatable blood pressure cuff was wrapped around a 10.18 cm diameter rigid cylinder. An elastic fabric (Performance Nylon & Spandex Fabric) was wrapped tightly on top of the pressure cuff underneath the

designed compression tourniquet to inflatable and deflate the cuff faster. A Cotton-based heat-protective layer was placed between the actuators and the cylinder to protect the cuff and the elastic fabric from heat damage. Throughout the experiments, the initial pressure of the cuff (and consequently the cylinder circumference) was manually adjusted by a squeeze bulb, and the inner pressure of the cuff was monitored by the pressure gauge. To provide the feedback for the controller and measure the pressure inside the pressure cuff, a low-pressure bidirectional gas pressure sensor (OMEGA PX242A-060G5V), previously used in [11], was placed between the pressure gauge and the inflatable cuff to record the pressure changes. The input voltage was set to 7.4 V using a DC power supply (Dr. Meter HY3005F-3), to regulate the sensor output voltage and achieve the proper accuracy for the pressure measurement ranges (20 – 90 mmHg). An Arduino Uno microcontroller was responsible for sampling the sensor output at 100 Hz and transferring the data through the Serial UART RS-232 protocol to the computer to be analyzed and fed into the designed PID controller running in MATLAB 2018. A KEITHLEY 2230G-30-6 power supply was used to provide the variable electrical power (current (A)) for activating the SMA actuators. This power supply has three programmable channels and can be controlled through Serial UART RS-232 or the National Instruments® VISA-USB interfaces. In either way, voltage and current levels could be set and fetched in real-time.

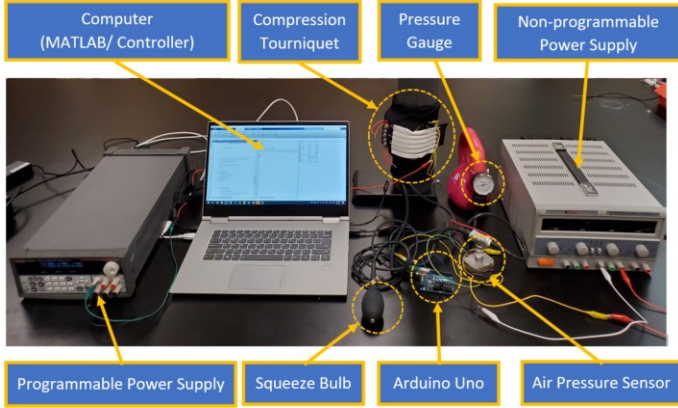


Figure 3: The experimental setup, including the developed prototype, control equipment (microcontroller, MATLAB, and power supplies), and the measurement devices (inflatable pressure cuff, sensors)

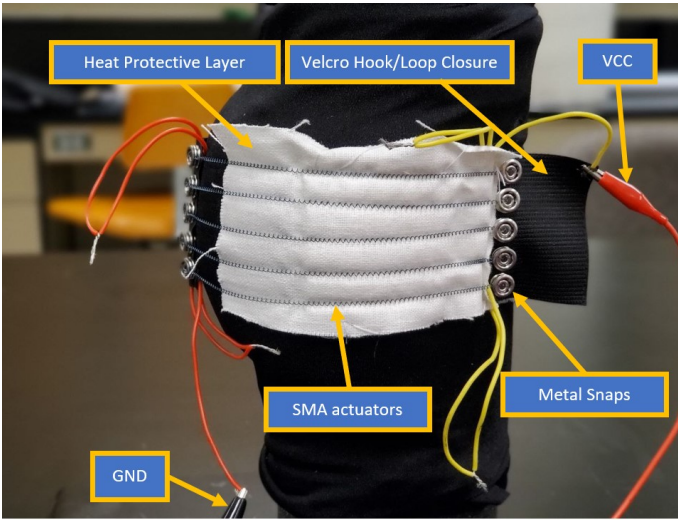


Figure 4: The developed SMA-based compression garment wrapped around a rigid cylinder while the pressure cuff was inflated

3. CHARACTERIZATION AND MODELING

3.1 Counter-pressure model development

In order to estimate the desired length of the actuators and evaluate the counter-pressure produced by the compression tourniquet, the model developed by Holschuh et al. [8] was adopted. According to this model, the maximum force for a low spring index coil actuator is calculated from:

$$F_{max} = \frac{G_A d^2}{8C^3 \eta} \epsilon \quad (1)$$

where, G_A is the material shear modulus in austenite (hot) phase, d is the SMA wire diameter, and C , η , ϵ are the spring index, packing density, and actuator extensional strain, respectively, which are obtained from the equations (2) to (4). In these equations, L_s is solid spring length, defined as the length of a spring that is fully packed, L_0 is free spring length, defined as the zero-load length of the spring (length of the SMA actuator when

fully actuated with no load), δ is the displacement, and D_i is the inner (core) diameter:

$$C = 1 + \frac{D_i}{d} \quad (2)$$

$$\eta = \frac{L_s}{L_0} \quad (3)$$

$$\epsilon = \frac{\delta}{L_0} \quad (4)$$

After calculating the maximum producible force for each actuator, the counter pressure (P) over a radius (r) of a cylindrical shape, such as a limb, is calculated based on the thin-walled hoop stress equation [16]:

$$P < \frac{Fn_{actuator}}{wr} \quad (5)$$

where w is the axial width of the compression element. Replacing the radius (r) with the circumference ($CI = 2\pi r$) equation results in the following counter-pressure equation:

$$P < \frac{2\pi Fn_{actuator}}{w CI} \quad (6)$$

Updating Eq. (6) with the real-world values of $G = 30 \times 10^9 Pa$, $d = 0.304 \times 10^{-3} m$, $D_i = 1.0414 \times 10^{-3} m$, the counter-pressure is obtained as:

$$P < \frac{125.60}{CI L_s w} \delta \quad (7)$$

As mentioned previously, button snaps have been used to provide a reliable connection between the garment and the actuators. The diameter of the snaps is 0.95 cm. Since there are five snaps used, in order to avoid circuit-shorting, a 3mm distance was placed between each snap. Therefore, the width of the tourniquet (w) was 6 cm. By choosing $L_s = 34 mm$ and $L_0 = 42 mm$, Eq (6) becomes:

$$P < \frac{61569.357}{CI} \delta \quad (7)$$

In order to find the relationship between the inner cuff pressure (P_c) and the changes in the cylinder's circumference (CI), 11 measurements were taken from 0 to 100 mmHg. From Figure 5, the following quadratic equation was fitted to the data with the Root Mean Square Error (RMSE) of 0.75 cm:

$$CI [cm] = -0.0004 P_c^2 + 0.1253 P_c + 37.98 \quad (8)$$

Therefore, by updating Eq. (7) with CI equation:

$$P < 6.1569 \times 10^4 \times \frac{[(-0.0004 P_c^2 + 0.1253 P_c + 37.98) \times 10^{-2} - L_e - L_0]}{(-0.0004 P_c^2 + 0.1253 P_c + 37.98) \times 10^{-2}} \quad (9)$$

Where $24\text{ cm} < L_e$ is the effective length of the tourniquet, which can be adjusted manually to take care of the intra- and inter-personal variabilities and ranges from 24 cm to 35 cm; and L_0 is the free spring length.

Putting $P_c = 50\text{ mmHg}$ and $L_e = 24\text{ cm}$ and $L_0 = 42\text{ mm}$ in Eq. (9) the equation becomes:

$$P < 2.1420 \times 10^4 \quad (10)$$

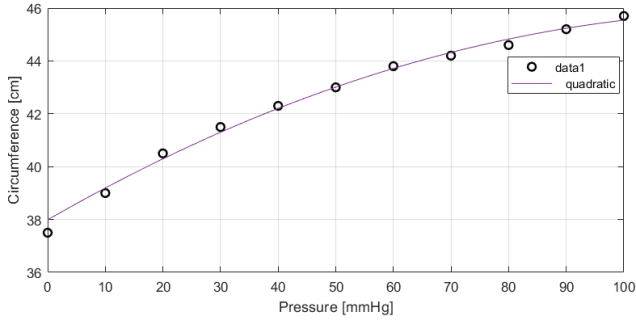


Figure 5: Pressure-Circumference measurements and the fitted quadratic model

3.2 Sensor Pressure Calibration

To find the relationship between the pressure analog sensor readout and the actual air pressure inside the cuff (P_c), air was pumped into the cuff manually using the squeeze bulb, and the value of the Arduino UNO 10-bit Analog-Digital-Converter (ADC) readout was monitored. In total, 34 measurements were taken within the range of 24 mmHg to 90 mmHg (Figure 6). From the data shown in this plot, the linear model could properly estimate the cuff pressure inside the cuff from the sensor ADC values. The equation for this linear model is:

$$P_c = 0.28736 \times \text{SensorADC} - 197.63 \quad (10)$$

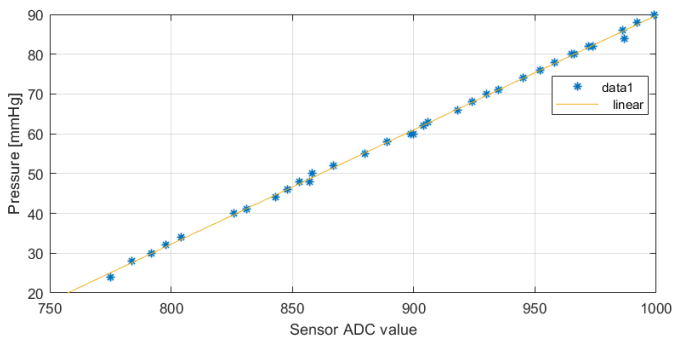


Figure 6: Sensor ADC vs. Actual inner cuff pressure

3.3 Sensor Drift

Drift is a phenomenon that commonly happens for sensors, especially where textiles are integrated into a compression or

sensing system [13]. Drift refers to sensor responses that exhibit changes over time, even in the absence of any external stimuli. Characterizing sensor drift is essential as it may drastically affect the results. Sensor drift occurs due to various reasons, which could be related to the nature of the sensor or other issues such as failure in the system or ambient effects [17]. Here, to characterize the system's pressure drift, the pressure cuff was inflated to 90 mmHg, and the pressure sensor measurement was monitored for 30 minutes. As shown in Figure 7 over a period of 30 minutes, the cuff pressure gradually decreased to 24.79 mmHg. This might happen due to a leak in the pneumatic system or the fabric relaxation (i.e., elasticity loss over time). In real-world situations this might be problematic and the mechanism causing the drift (system leakage or sensor drift) should be identified prior to the experiments. However, this study lumps the change in pressure over time in a single pressure drift value. Here, we intentionally left the drift problem to remain, as it represents uncertainty in the system and allows us to determine the efficacy and robustness of the controller in overcoming this challenge which is central to textile-based wearable technologies.

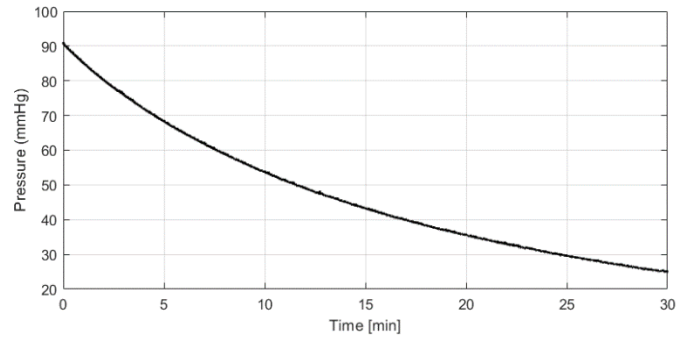


Figure 7: System pressure drift over time (30 minutes)

4. CLOSED-LOOP PRESSURE CONTROL

4.1 Actuator Force-Current Analysis

To characterize the behavior of the actuators while being stimulated by the Joule heating approach, the Instron 3365 Series Universal Testing System was used. To this end, an actuator with L_s and L_0 of 34 mm and 42 mm, respectively, was held at an extensional strain (δ) of 112 mm ($\epsilon(\%) = 266\%$). The actuator was heated using Joule heating by connecting it to the VCC and GND of the programmable power supply. The current limit was incrementally increased by 50 mA, 25 seconds per step. As shown in Figure 8 no significant change in force was observed before (200 mA) due to the fact that the actuators were not sufficiently heated enough to cross the critical activation temperature (70°C for the specific type of SMAs used in this study, Flexinol 0.304mm thickness). For all currents greater than 300mA, force increased progressively. At 1150 mA, the average force profile started decreasing, indicating that austenite activation has been completed. At this point, as a result of

overheating, shape setting condition occurs, meaning that the SMA material memory is reset, and it is no longer able to generate active force and actuate as expected. From the design and control perspective, this point is critical as we should not exceed this current limit to avoid overheating the actuators, which leads to a loss in shape memory and active force.

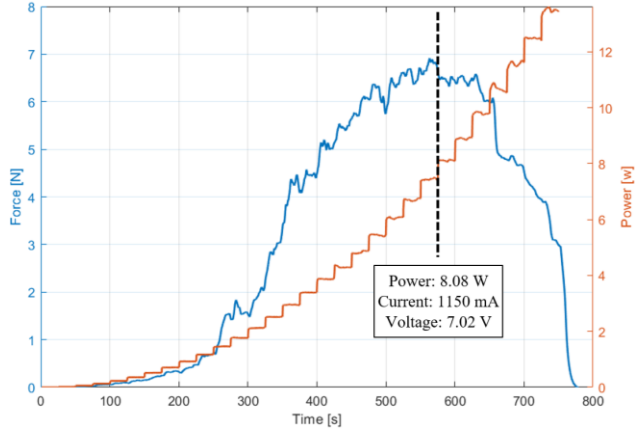


Figure 8: The Force-Power (w) curves for an SMA actuator ($\delta = 112$ mm) demonstrating the power/current threshold for activating the actuators

4.2 Controller Design

To control the tourniquet compression, a PID controller was adopted, which has been proven to be a robust and reliable controller for controlling SMA spring actuation [18]. The block diagram of the implemented controller is shown in Figure 9. In this controller, current was chosen as the system input and the cuff compression as the output. In order to avoid overheating the actuators, the input saturation (u_{sat}) was set to 900 mA which is below the maximum allowable current value, 1150 mA.

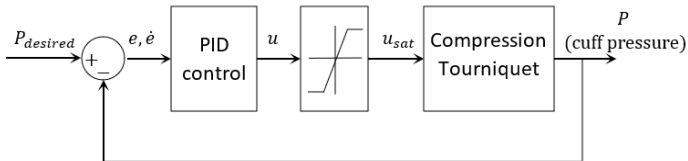


Figure 9: The implemented PID controller block diagram

To achieve the optimum rise time, settling time, steady-state error, the PID gains were adjusted heuristically, and the performance of the controller was evaluated. The effect of trying different PID gains (K_p , K_i , K_d) for controlling the inner cuff pressure has been plotted in Figure 10 from between $t = 3$ s and 160 s. In this 3-minute test, the pressure inside the cuff was initially set to 96 mmHg, and the desired pressure for the controller was set to 110 mmHg. As shown in this figure, based on the system response, the PID controller with gains of $k_p = 0.26$, $k_i = 0.03$, and $k_d = 0.01$ performs relatively better than the other controllers in terms of settling time, steady-state error, rise time, and electrical power consumption. The average final value (calculated for the last 60 seconds), rise time, and settling time for this controller were 109 mmHg, 4.63 s, and 15 s,

respectively. Therefore, these gains were chosen as the PID controller gains to conduct further experiments.

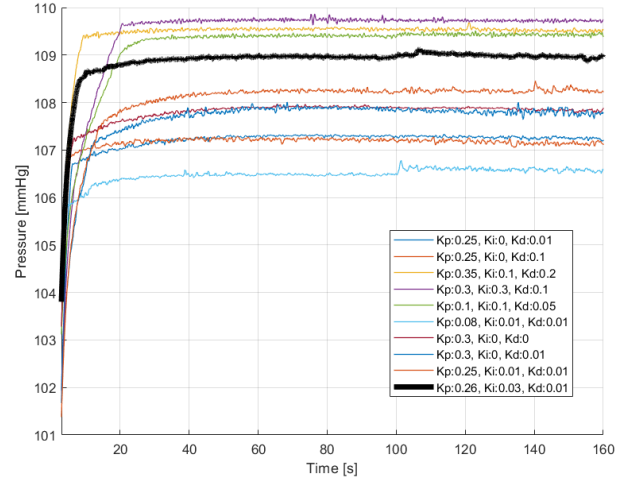


Figure 10: PID gain adjustment for the controller ($K_p:0.26$, $K_i:0.03$, and $K_d:0.01$, were chosen as the final controller gains)

5. TESTING PROCEDURE

To evaluate the performance of the compression system in generating the desired pressure levels, five types of experiments were carried out:

- **Incremental compression test:** Assessing the ability of the compression tourniquet to generate the pressure at incremental levels without recovery (Figure 11).
- **Variable compression test:** Investigating the ability of the compression tourniquet to generate variable pressure levels (Figure 12).
- **Cyclic test:** Investigating the system capacity in generating the variable pressure levels in a cyclic manner (Figure 13).
- **Compression maintenance test:** Investigating the capability of the designed compression system in maintaining the compression for longer periods (Figure 14).
- **Fixed-step test:** Investigating the compression rate and the maximum producible pressure by the tourniquet (Figure 15).

Although the aforementioned tests were primarily designed to characterize and evaluate the performance of the fabricated dynamic compression tourniquet and the controller system, from the medical perspective, these tests can also represent the different types of compression modes that are used in medical compression therapy. For instance, fixed-step and compression maintenance tests have been designed based on the compression bandages and stockings mechanisms that are supposed to apply a static pressure on the body for a specific period of time. Also, the cyclic test has been designed to simulate the mechanism of the Intermittent Pneumatic Compression (IPC) devices. IPC, is another form of compression that does not involve bandaging and known as one of the effective mechanisms in reducing fibrosis and enhancing ulcer healing [19,20]. IPC devices consist of an air pump that periodically inflates and deflates a bladder to compress the leg to a preset pressure level [19]. The desired

pressure profiles corresponding to each test are shown in Figure 11 to Figure 15. Except for the fixed-step test (which was done once due to the actuation loss), each test was repeated three times to assess the repeatability of the garment compression generation.

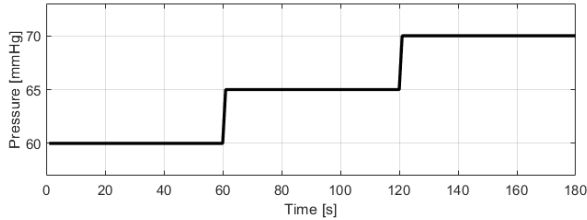


Figure 11: Incremental compression test desired pressure path for the controller

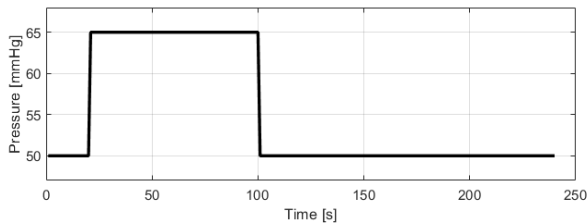


Figure 12: Variable compression test desired pressure path for the controller

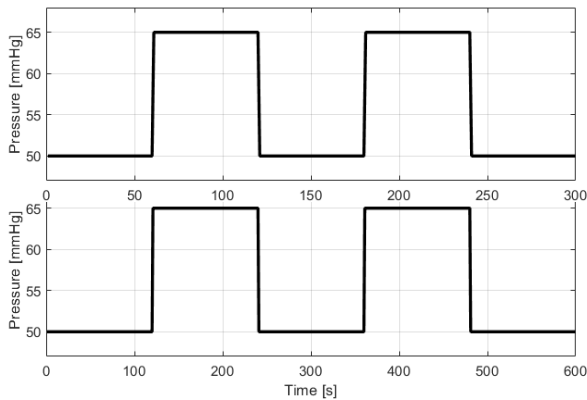


Figure 13: Cyclic test desired pressure path for the controller

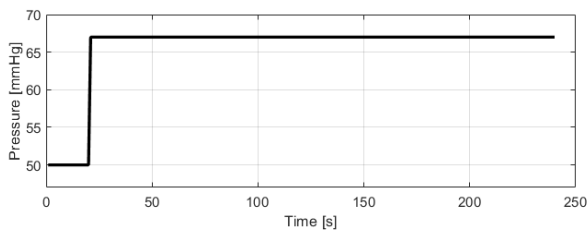


Figure 14: Compression maintenance test desired pressure path for the controller

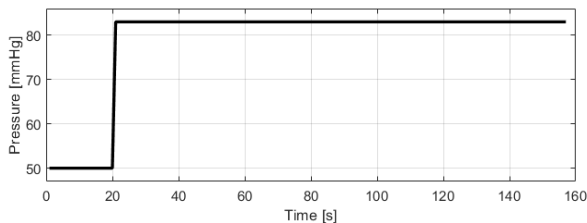


Figure 15: Fixed-step test desired pressure path for the controller

6. RESULTS AND DISCUSSION

The results corresponding to the tests discussed in the previous section are shown in Figure 16 to Figure 21. In addition to the control results, to better understand the ability of the tourniquet to control compression, the normal behavior of the sensing system (when the tourniquet is not put on), which was introduced as system pressure drift earlier, has been visualized. The performance of the system was evaluated under the five conditions previously described.

6.1 Incremental compression test results and discussion

Figure 16 demonstrates the results corresponding to the incremental experiments in which the desired pressure trajectory was set to rise in three steps, starting from 50 mmHg to 60 mmHg, 60 mmHg to 65 mmHg, and 65 mmHg to 70 mmHg. As shown, the compression tourniquet is able to follow the desired pressure pattern with the expected steady-state error of ~ 1 mmHg (which is due to the PID gains chosen, discussed in the previous sections). It should be mentioned that this steady-state error could be decreased by adjusting the PID gains, especially the integral gain (k_i), however an increase in settling time would be expected. Moreover, from this figure, and all the following figures, it is evident that the controller can overcome the pressure drift that exists in the system (see Figure 7) such that the difference between the cuff pressure and the normal behavior of the pressure system reaches up to more than 24 mmHg. The other noticeable point about this figure is the consistency between the first two steps of the trials and the slight creep in the third trial. This actually represents one of the challenges of using soft materials, where the soft actuators might migrate on a soft surface such as skin (and here, fabric), which causes some variations between the trials. This figure also emphasizes the importance of the closed-loop controller in dealing with the

disturbances or uncertainties caused by soft materials in the system.

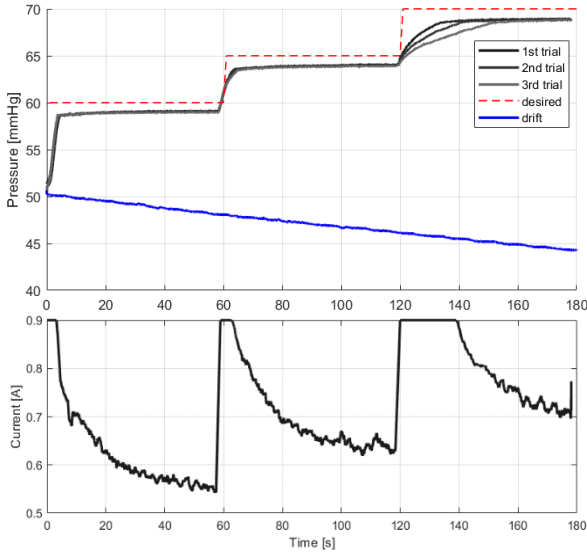


Figure 16: Incremental compression test results (top) and the corresponding control effort (Current [A]) (bottom)

6.2 Variable compression test results and discussion

The second experiment was done in order to investigate the ability of the compression tourniquet to generate variable pressure levels, as can be seen in Figure 17. In this test, the desired pressure reference was set to 50 mmHg and increased by 15 mmHg after 20 seconds, after which it stayed at this level for 80 seconds. Then the reference pressure was dropped again to 50 mmHg and remained at this level for 140 seconds to the end of the test. As can be seen, the controller performed well in preserving the pressure amount at this level. Although drift was expected, the controller prevented the pressure from being affected by increasing the control effort (i.e., increasing the current limit (A)), as demonstrated in Figure 7. As seen in this figure, the control input was saturated at the maximum allowable current level of 900 mA between 20 and 40 seconds. Once the SMAs' temperature reached the point that 64 mmHg could be provided by the tourniquet actuators, the current was gradually decreased and stabilized at ~0.6 A to maintain the desired pressure. When a lower pressure was desired, the controller eliminated the power to the system until the lower pressure was reached. Therefore, within the period of 100s to 172s, the current was set to the lowest possible amount to let the actuators cool down and recover to the martensite phase as fast as possible. Once the pressure dropped to 49 mmHg, the current was input to the system to maintain the pressure at the desired level. The noticeable point here is that the control effort has roughly

increased by 80 mA after $t = 187s$ to overcome the pressure drift.

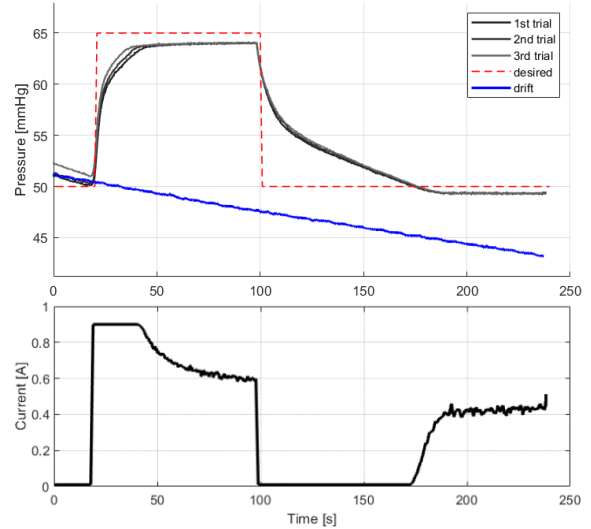


Figure 17: (top) Variable compression test results and (bottom) the corresponding control effort (plotted for the first trial)

6.3 Cyclic test results and discussion

The third experiment was conducted to investigate the performance of the compression system in generating the desired level of pressure after recovering to lower pressure in a cyclic manner. As explained before, the compression tourniquet was set to follow a cyclic desired path shown in Figure 18 and Figure 19, in which the bottom-line and top-line pressures are 50 and 65 mmHg. In the first test, the recovery period was minimized, and the tourniquet was activated immediately after it reached the bottom-line pressure (~1 minute), while in the second experiment, the recovery phase lasted 2 minutes to let the tourniquet recover enough before highly activating by larger current levels. According to the test results shown in Figure 18 and Figure 19, in both cases, the controller performed well and activated the actuators through Joule heating by regulating the current limit (A) to make the tourniquet follow the desired cyclic pattern. It is worth mentioning that longer hold times at the bottom-line (low pressure) and top-line (high pressure) did not affect the recovery and actuation times, respectively, at the range in time scales tested. In both experiments, the actuation and recovery were similar and found to be 22 seconds and 45 seconds

approximately. Also, the expected steady-state error of 1 mmHg was observed.

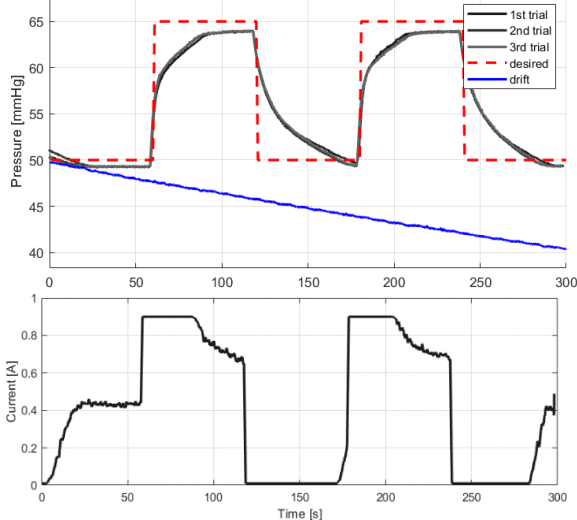


Figure 18: (top) Cyclic test results of the 1st experiment [activation period: 1 min, recovery period: 1 min] and (bottom) the corresponding control effort (plotted for the first trial)

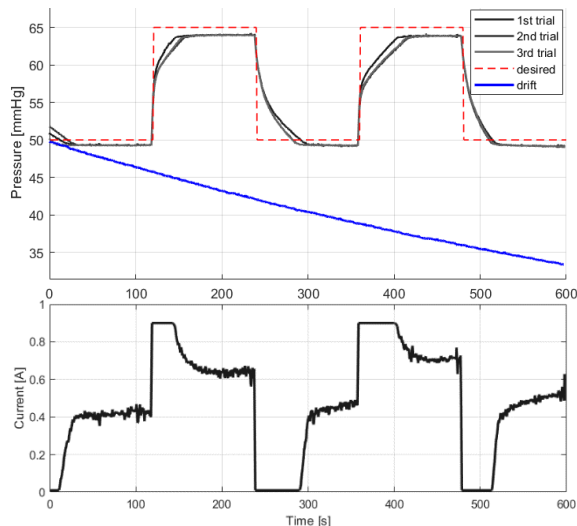


Figure 19: (top) Cyclic test results of the 2nd experiment [activation period: 2 min, recovery period: 2 min] and (bottom) the corresponding control effort (plotted for the first trial)

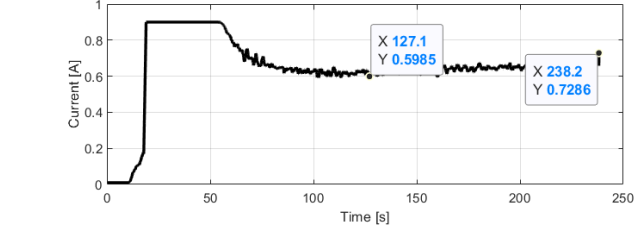
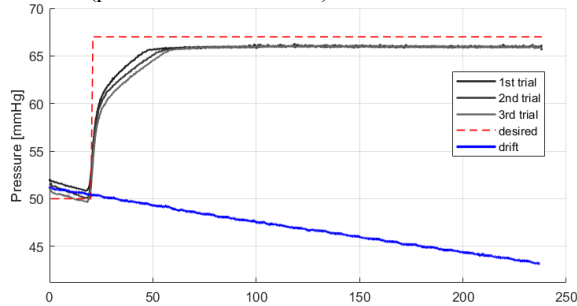


Figure 20: (top) Compression maintenance test results and (bottom) the corresponding control effort (plotted for the first trial)

6.4 Compression maintenance test results and discussion

In the fourth experiment, the system's capability in maintaining compression for a more extended period was studied. The desired compression was set to 50 mmHg for 20 seconds then 67 mmHg for 220 seconds. The compression was adjusted by the SMA actuators to successfully follow the desired pressure path. As shown in Figure 20, the controller has properly regulated the input current to control the temperature of the actuators to successfully follow the desired pressure path and adjust to the pressure drift. For instance, the electrical current and the power consumption have increased by 22% (from 0.59 A to 0.72 A) between $t = 127s$ and $t = 238s$. The average current increase for this interval is 46mA.

6.5 Fixed step test results and discussion

The last experiment was carried out to measure the maximum producible compression generated by the garment and to investigate the compression rate (mmHg/s). Compression rate is an important factor for some applications such as intermittent compression therapy in which the compression is applied at specific time intervals, which could be set through a fixed or smart timing algorithms [21]. To measure the compression rate, the entire test duration from $t = 20s$ to $t = 167s$ was split into 10-second intervals, and the rate was calculated in a piecewise fashion. The compression rates are summarized in Table 1. According to this table and Figure 21, the maximum rate of 1.26 mmHg/s was achieved between $t = 20s$ and $t = 30s$. However, the actuation speed dropped considerably to 0.2 mmHg/s within $t = 30s$ and $t = 40s$. The same pattern occurs in the later periods such that the actuation speed nonlinearly decays and reaches 0.05 mmHg/s at the end of the test. Throughout the experiment, the average compression is calculated as 0.19 mmHg/s while the control effort, current, was saturated at 0.9 A. Moreover, given the system pressure drift and the fact that the compression generated by the tourniquet was still increasing at the end of the experiment at $t = 167s$, it can be concluded that the designed compression garment is able to generate more than 33 mmHg, which is calculated as the difference between the drift and the test curves at $t = 167s$.

Table 1: The rates of compression generated by the tourniquet within 10-second intervals from $t = 127s$ to $t = 238s$

Time (s)	20-30	30-40	40-50	50-60	60-70	70-80	80-90	90-100
----------	-------	-------	-------	-------	-------	-------	-------	--------

Range (mmHg)	[50-62.68]	[62.68-64.7]	[64.7-66.40]	[66.40-67.95]	[67.95-69.34]	[69.34-70.65]	[70.65-71.91]	[71.91-73.07]	
Rate (mmHg/s)	1.26	0.20	0.16	0.15	0.14	0.13	0.12	0.11	
Time (s)	100-110	110-120	120-130	130-140	140-150	150-160	160-167		Average
Range (mmHg)	[73.07-74.07]	[74.07-74.96]	[74.96-75.87]	[75.87-76.69]	[76.69-77.46]	[77.46-77.99]	[77.99-78.37]		
Rate (mmHg/s)	0.10	0.08	0.09	0.08	0.07	0.05	0.05	0.19	

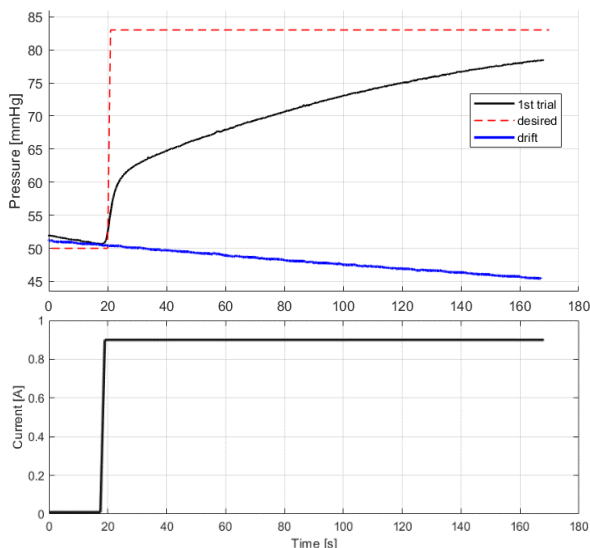


Figure 21: (top) Fixed-step test results and (bottom) the corresponding control effort

7. CONCLUSION

This paper documents the development of an SMA-based smart tourniquet capable of producing a controllable pressure of more than 33 mmHg for circumferential applications. This smart tourniquet is 6 cm wide and uses a modular design to meet 99th percentile leg size at the maximum circumference. To assess the tourniquet's performance, a pneumatic-based sensor system was developed, including an inflatable pressure cuff wrapped around a rigid cylinder and a gas pressure sensor. The thermal activation of the SMA actuators was controlled by a PID controller through the Joule heating approach. The PID gains were adjusted to achieve the best settling time, rise time, stability, steady-state error, and power consumption. A controllable power supply was used to provide the variable input to the system. After choosing the proper gains for the controller, five different experiments were carried out to investigate the ability of the compression system to generate variable pressure levels. These experiments showed that the designed tourniquet and the implemented PID controller can effectively adapt compression to accommodate the pressure drift that exists in the system. Also, the controller can adjust the current (A) (as the input) so that the desired pressure task was successfully achieved within the steady-state error of 1 mmHg. Furthermore, the test results revealed that the actuation rate could adapt to variations in the cylinder circumference and the internal pressure of the cuff ranging from 1.25 mmHg/s

(between 50 and 62.68 mmHg) to 0.05 mmHg/s (between 77.99-78.37 mmHg), with an average of 0.19 mmHg/s. Part of this relatively low actuation rate could be related to the inherent low-speed actuation of the SMA materials. However, it may also be influenced by the friction between the tourniquet and cylinder surface. In the future, other materials could be used in order to reduce friction. Also, to improve the control results, other linear and nonlinear controllers could be applied to the system. Moreover, in future studies, the soft textile-based sensors could be used to better simulate on-body sensing conditions. This research establishes accurate closed-loop control of SMA-incorporated compression technology, which has the potential to enable diverse devices that require a controlled amount of pressure to be applied on the body, such as medical therapy, cosmetics, athletics, and aerospace engineering.

ACKNOWLEDGEMENT

The authors would like to thank their classmates for their helpful suggestions made through the peer-review process in ME8243 Topics in Design: Advanced Materials class at the University of Minnesota. This work was supported by the US National Science Foundation under grants #1722738 and #1943715.

REFERENCES

- [1] Liu, R., Guo, X., Lao, T. T., and Little, T., 2017, "A Critical Review on Compression Textiles for Compression Therapy: Textile-Based Compression Interventions for Chronic Venous Insufficiency," *Text. Res. J.*
- [2] Webb, P., and Annis, J. F., 1967, "The Principle of the Space Activity Suit. NASA CR-973.," NASA Contract. Rep. NASA CR.
- [3] Waldie, J. M. A., Tanaka, K., Tourbier, D., Webb, P., Jarvis, C. W., and Hargens, A. R., 2002, "Compression under a Mechanical Counter Pressure Space Suit Glove.," *J. Gravit. Physiol.*
- [4] Figueroa, J. J., Singer, W., Sandroni, P., Sletten, D. M., Gehrking, T. L., Gehrking, J. A., Low, P., and Basford, J. R., 2015, "Effects of Patient-Controlled Abdominal Compression on Standing Systolic Blood Pressure in Adults with Orthostatic Hypotension," *Arch. Phys. Med. Rehabil.*
- [5] Platts, S. H., Tuxhorn, J. A., Ribeiro, L. C., Stenger, M. B., Lee, S. M. C., and Meck, J. V., 2009, "Compression Garments as Countermeasures to Orthostatic Intolerance," *Aviat. Sp. Environ. Med.*
- [6] Gonçalves, C., da Silva, A. F., Simoes, R., Gomes, J., Stirling, L., and Holschuh, B., 2019, "Design and Characterization of an Active Compression Garment for the Upper Extremity," *IEEE/ASME Trans. Mechatronics.*
- [7] Holschuh, B., and Newman, D., 2014, "Low Spring Index, Large Displacement Shape Memory Alloy (Sma) Coil Actuators for Use in Macro-and Micro-Systems," *Reliability, Packaging, Testing, and Characterization of*

- MOEMS/MEMS, Nanodevices, and Nanomaterials XIII*, International Society for Optics and Photonics, p. 897505.
- [8] Holschuh, B., Obropta, E., and Newman, D., 2015, “Low Spring Index NiTi Coil Actuators for Use in Active Compression Garments,” *IEEE/ASME Trans. Mechatronics*.
- [9] Granberry, R., Eschen, K., Holschuh, B., and Abel, J., 2019, “Functionally Graded Knitted Actuators with NiTi-Based Shape Memory Alloys for Topographically Self-Fitting Wearables,” *Adv. Mater. Technol.*
- [10] Eschen, K., Abel, J., Granberry, R., and Holschuh, B., 2018, “Active-Contracting Variable-Stiffness Fabrics for Self-Fitting Wearables,” *ASME 2018 Conference on Smart Materials, Adaptive Structures and Intelligent Systems, SMASIS 2018*.
- [11] Beldon, P., 2008, “Compression Bandaging: Avoiding Pressure Damage.,” *Br. J. Community Nurs.*
- [12] Golgouneh, A., Holschuh, B., Compton, C., and Dunne, L. E., 2021, “Evaluation of Textile-Based Wearable Force Sensors for Functional Clothing Applications.”
- [13] Golgouneh, A., Tahmidul Islam Molla, M., and Dunne, L. E., 2019, “A Comparative Feasibility Analysis for Sensing Swelling with Textile-Based Soft Strain Sensors,” *Proceedings - International Symposium on Wearable Computers, ISWC*.
- [14] O’Brien, B., Gisby, T., and Anderson, I. A., 2014, “Stretch Sensors for Human Body Motion,” *Electroactive Polymer Actuators and Devices (EAPAD) 2014*.
- [15] Grattan, K. T. V., and Meggit, B. T., 2000, *Optical Fiber Sensor Technology Advanced Applications - Bragg Gratings and Distributed Sensors*.
- [16] Judnick, D., Newman, D., and Hoffman, J., 2007, “Modeling and Testing of a Mechanical Counterpressure Bio-Suit System,” *SAE Technical Papers*.
- [17] Abe, M., Sugimoto, Y., Namikawa, T., Morita, K., Oyabu, N., and Morita, S., 2007, “Drift-Compensated Data Acquisition Performed at Room Temperature with Frequency Modulation Atomic Force Microscopy,” *Appl. Phys. Lett.*
- [18] Golgouneh, A., Holschuh, B., and Dunne, L., 2020, “A Controllable Biomimetic SMA-Actuated Robotic Arm,” *Proceedings of the IEEE RAS and EMBS International Conference on Biomedical Robotics and Biomechatronics*.
- [19] Allenby, F., Pflug, J. J., Boardman, L., and Calnan, J. S., 1973, “EFFECTS OF EXTERNAL PNEUMATIC INTERMITTENT COMPRESSION ON FIBRINOLYSIS IN MAN,” *Lancet*, 302(7843), pp. 1412–1414.
- [20] Tarnay, T. J., Rohr, P. R., Davidson, A. G., Stevenson, M. M., Byars, E. F., and Hopkins, G. R., 1980, “Pneumatic Calf Compression, Fibrinolysis, and the Prevention of Deep Venous Thrombosis,” *Surg. (United States)*.
- [21] Fawcett, A., 2018, “The Influence of Timing on the